Detecting multiparticle entanglement of Dicke states

Bernd Lücke[1], Jan Peise[1], Giuseppe Vitagliano[2], Jan Arlt[3], Luis Santos[4], Géza Tóth[2,5,6], Carsten Klempt[1]

[1]*Institut für Quantenoptik, Leibniz Universität Hannover, Welfengarten 1, D-30167 Hannover, Germany*
[2]*Department of Theoretical Physics, University of the Basque Country UPV/EHU, P.O. Box 644, E-48080 Bilbao, Spain*
[3]*QUANTOP, Institut for Fysik og Astronomi, Aarhus Universitet, 8000 Århus C, Denmark*
[4]*Institut für Theoretische Physik, Leibniz Universität Hannover, Appelstraße 2, D-30167 Hannover, Germany*
[5]*IKERBASQUE, Basque Foundation for Science, E-48011 Bilbao, Spain and*
[6]*Wigner Research Centre for Physics, H. A. S., P.O. Box 49, H-1525 Budapest, Hungary*
(Dated: September 11, 2014)

Recent experiments demonstrate the production of many thousands of neutral atoms entangled in their spin degrees of freedom. We present a criterion for estimating the amount of entanglement based on a measurement of the global spin. It outperforms previous criteria and applies to a wide class of entangled states, including Dicke states. Experimentally, we produce a Dicke-like state using spin dynamics in a Bose-Einstein condensate. Our criterion proves that it contains at least genuine 28-particle entanglement. We infer a generalized squeezing parameter of $-11.4(5)$ dB.

Entanglement, one of the most intriguing features of quantum mechanics, is nowadays a key ingredient for many applications in quantum information science [1, 2], quantum simulation [3, 4] and quantum-enhanced metrology [5]. Entangled states with a large number of particles cannot be characterized via full state tomography [6], which is routinely used in the case of photons [7, 8], trapped ions [9], or superconducting circuits [10, 11]. A reconstruction of the full density matrix is hindered and finally prevented by the exponential increase of the required number of measurements. Furthermore, it is technically impossible to address all individual particles or even fundamentally forbidden if the particles occupy the same quantum state. Therefore, the entanglement of many-particle states is best characterized by measuring the expectation values and variances of the components of the collective spin $\mathbf{J} = (J_x, J_y, J_z)^T = \sum_i \mathbf{s}_i$, the sum of all individual spins $\mathbf{s}_i$ in the ensemble. In particular, the spin-squeezing parameter $\xi^2 = N \frac{(\Delta J_z)^2}{\langle J_x \rangle^2 + \langle J_y \rangle^2}$ defines the class of spin-squeezed states for $\xi^2 < 1$. This inequality can be used to verify the presence of entanglement, since all spin-squeezed states are entangled [12]. Large clouds of entangled neutral atoms are typically prepared in such spin-squeezed states, as shown in thermal gas cells [13], at ultracold temperatures [14–16] and in Bose-Einstein condensates [17–19].

Systems with multiple particles may exhibit more than pairwise entanglement. Multiparticle entanglement is best quantified by means of the so-called entanglement depth, defined as the number of particles in the largest non-separable subset [see Fig. 1 (a)]. There have been numerous experiments detecting multiparticle entanglement involving up to 14 qubits in systems, where the particles can be addressed individually [9, 20–24]. Large ensembles of neutral atoms pose the additional challenge of obtaining the entanglement depth from collective measurements. Following the criterion for k-particle entanglement of Ref. [25], multiparticle entanglement has been experimentally demonstrated in spin-squeezed
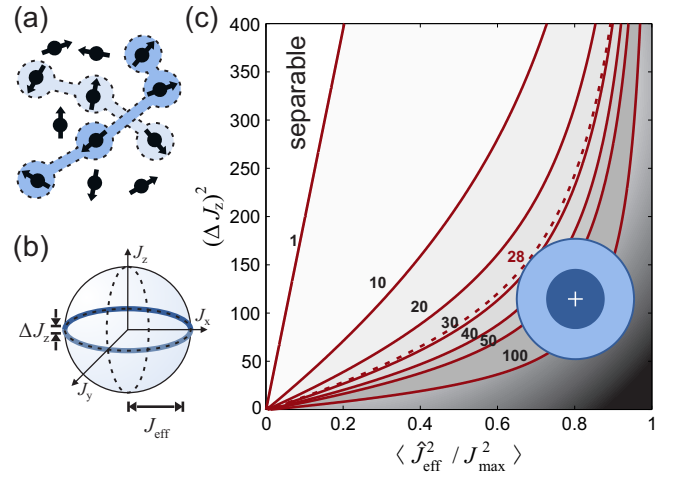

FIG. 1. Measurement of the entanglement depth for a total number of 8000 atoms. (a) The entanglement depth is given by the number of atoms in the largest non-separable subset (shaded areas). (b) The spins of the individual atoms add up to the total spin $\mathbf{J}$ whose possible orientations can be depicted on the Bloch sphere. Dicke states are represented by a ring around the equator with an ultralow width ΔJ_z and a large radius J_{eff}. (c) The entanglement depth in the vicinity of a Dicke state can be inferred from a measurement of these values. The red lines indicate the boundaries for various entanglement depths. The experimental result is shown as blue uncertainty ellipses with one and two standard deviations, proving an entanglement depth larger than 28 (dashed line).

Bose-Einstein condensates [17]. However, the method only applies to spin-squeezed states, which constitute a small subset of all possible entangled many-particle states. Moreover, the strong entanglement of states with extreme sub-shot-noise fluctuations is not detected under influence of minimal experimental noise [26]. Whereas entanglement detection for more general entangled states has already been developed [27, 28], it is desirable to extend these methods towards the detection of multiparti-

cle entanglement.

In this Letter, we introduce a method for the quantification of entanglement. Our criterion is applicable to both spin-squeezed and more extreme states, yielding superior results compared to the inspiring work by Sørensen/Mølmer [25] and Duan [29]. It enables us to quantify the multiparticle entanglement of an experimentally created Dicke-like state, yielding a minimum entanglement depth of 28. In addition, we extract a generalized squeezing parameter, which is also applicable to Dicke states, of $-11.4(5)$ dB, so far the best reported value in any atomic system.

Dicke states [30] constitute a particularly relevant class of highly entangled, but not spin-squeezed states. They are simultaneous eigenstates $|J, M\rangle$ of $\mathbf{J}^2$ and J_z, and the spin-squeezing parameter ξ^2 does not detect them as entangled [31]. Nonetheless, Dicke states have optimal metrological properties [32–34] and can be used to reach Heisenberg-limited sensitivity [35]. They are also useful for quantum information processing tasks, such as $1 \rightarrow (N - 1)$ telecloning or open-destination teleportation [36]. Experimentally, high-fidelity Dicke states with small particle numbers have been created with photons [22, 23] and trapped ions [9], and have been detected by global measurements [37].

Among other methods [38, 39], large numbers of atoms in Dicke states with $|J, M = 0\rangle$ may be created in spinor Bose-Einstein condensates [40]. Spin dynamics creates a superposition of Dicke states with varying total number of particles in a process that resembles optical parametric down-conversion [41, 42]. In previous work, the entanglement of these states was proven by a homodyne measurement [43] and by a test of the metrological sensitivity beyond shot noise [44]. However, the achieved metrological sensitivity did not imply more than pairwise entanglement [34].

For the generation of the desired Dicke states, we prepare a ^{87}Rb Bose-Einstein condensate of 2×10^4 atoms in a crossed-beam dipole trap with trapping frequencies of $2\pi \times (200, 150, 150)$ Hz. Initially prepared in the Zeeman level $(F, m_F) = (1, 0)$, atoms collide and form correlated pairs in the two Zeeman levels $(1, \pm 1)$. These atoms are transferred to distinct spatial modes [41, 45], which are addressed by microwave dressing [40] the Zeeman level $(1, 1)$ [Fig. 2 (b)]. In an experimental run, up to $N = 8 \times 10^3$ atoms are transferred to the first excited mode along the strongest trap axis within 240 ms. Since they are transferred pairwise, we expect an equal number of atoms $N_{\pm 1} = \frac{N}{2}$ in the two Zeeman levels $(1, \pm 1)$. These atoms are highly entangled in analogy to optical parametric down-conversion. It is the central objective of this Letter to quantify the entanglement depth of the created many-particle state.

We restrict the description of the output state to the two relevant Zeeman levels $(1, \pm 1)$. In this pseudo-spin-$\frac{1}{2}$ system, we characterize the state by the collective spin
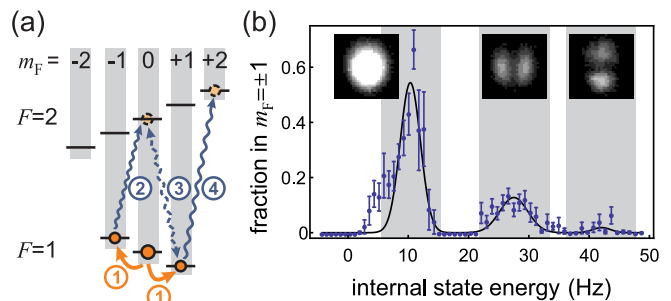

FIG. 2. Preparation and detection of a Dicke-like state. (a) A Bose-Einstein condensate in the level $(F, m_F) = (1, 0)$ generates clouds with the same number of atoms in the levels $(1, \pm 1)$ (1). A microwave pulse (2) transfers the atoms from $(1, -1)$ to $(2, 0)$. Optionally, a microwave pulse (3) can be used to couple the two clouds for the measurement of J_{eff}. Finally, the atoms in the level $(1, 1)$ are transferred to $(2, 2)$ before detection. (b) The number of atoms is measured by standard absorption imaging (insets). On well-resolved resonances depending on the internal state energy, distinct spatial modes are populated with a large fraction of the total number of atoms. The black line is a Gaussian fit to guide the eye. In our experiments, we use the resonance at ≈ 28 Hz.

$\mathbf{J}$, resulting from the sum of the individual pseudospins. In this picture, the ideal output state with equal number of atoms constitutes the Dicke state $\left|J = \frac{N}{2}, M = 0\right\rangle$ with vanishing fluctuations ΔJ_z. The fluctuations of the collective spin can be measured directly by counting the number of atoms in the two Zeeman levels. For this purpose, we transfer the atoms to the levels $(2, 0)$ and $(2, 2)$ with microwave pulses [see Fig. 2 (a)]. Subsequently, the trap is switched off and a strong magnetic field gradient separates the spin components during ballistic expansion. The number of atoms is then measured by standard absorption imaging. The absolute number of atoms was calibrated [44] and it was confirmed that shot noise fluctuations are observed for a coherent state [see Fig. 3 (a)], which was created by splitting a Bose-Einstein condensate with a $\frac{\pi}{2}$ microwave pulse.

We measure J_x and J_y by rotating the total spin using a $\frac{\pi}{2}$ microwave coupling pulse on the $(1, 1)$ to $(2, 0)$ transition before the number measurement [see Fig. 2 (a)]. Whether J_x or J_y is measured depends on the relation between the microwave phase and the phase of the initial Bose-Einstein condensate. The condensate phase represents the only possible phase reference in analogy to the local oscillator in optics. Intrinsically, it has no relation to the microwave phase, such that we homogeneously average over all possible phase relations in our measurements. For a given phase difference α, a rotation yields a measurement of $J_\alpha \equiv \cos\alpha J_x + \sin\alpha J_y$. Averaging over all possible α, the measured expectation value of the second moment corresponds to $\frac{1}{2\pi} \int_0^{2\pi} \langle J_\alpha^2 \rangle \mathrm{d}\alpha = \left\langle \frac{1}{2}(J_x^2 + J_y^2) \right\rangle$. After a random rotation, we thus record
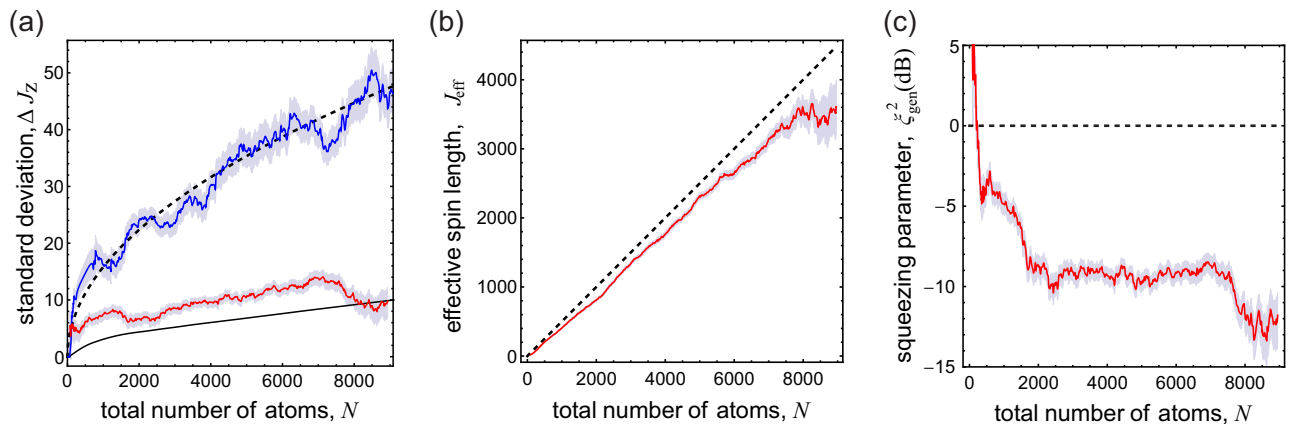
FIG. 3. Characterization of the experimentally created Dicke-like state. (a) Measurement of the width ΔJ_z for varying total number of atoms (red line). Each value and its statistical uncertainty (gray shading) is calculated for a 1000-atom interval within the total number of atoms. The measured values of ΔJ_z are well below the shot noise limit (theory: black dashed line, experiment: blue solid line) and partially explained by a lower limit of the number dependent detection noise (black solid line). (b) The measured value of J_{eff} as a function of the total number of atoms almost reaches its optimal value (black dashed line). The inset shows that the normalized J_{eff} is slowly reduced during an additional hold time. (c) The recorded data allows for a determination of the optimal spin-squeezing parameter as a function of the total number of atoms. At a total of 8000 atoms, it reaches a value of $-11.4(5)$ dB.

the effective spin length $J_{\text{eff}}^2 = \langle \hat{J}_{\text{eff}}^2 \rangle = \langle J_x^2 + J_y^2 \rangle$, which equals the spin length in the limit of vanishing $\langle J_z^2 \rangle$ [46]. Dicke states can be ideally characterized by the measurement of a large J_{eff} and a small variance $(\Delta J_z)^2$ [see Fig. 1 (b)].

Figure 3 (a) depicts the results of our measurement of ΔJ_z depending on the total number of atoms N. The recorded fluctuations were corrected for the independently measured detection noise of 10.9(3) atoms to obtain the pure atomic noise. The detection noise was directly extracted from images of the detection beams and is mainly caused by the photoelectron shot noise on the camera. The measured atom number fluctuations are well below the atomic shot noise level, reaching down to -12.4 ± 1.2 dB at a total number of 8000 atoms. The fluctuations are almost independent of the total number of atoms with a small trend of $0.15\sqrt{N}$. We do not record an increase of the measured fluctuations for a variable additional hold time of up to 420 ms. Thus, we can exclude three-body losses, collisions with the background gas or radio-frequency noise as relevant noise sources. We attribute the measured fluctuations to an additional detection noise since photoelectron shot noise and the influence of technical noise of the imaging beams are expected to increase slightly for a larger number of atoms. The solid line in Fig. 3 (a) shows an estimated lower limit of this effect [26].

A measurement of the effective spin length J_{eff} is presented in Fig. 3 (b). The values for J_{eff} almost reach their optimal value of $J_{\text{max}} = \frac{N}{2}$. This measurement shows that the created state is nearly fully symmetric. After a

variable hold time, the measured effective spin length diminishes slowly [see Fig. 3 (b), inset]. We thus conclude that the measurement result is limited by magnetic field gradients and collisions. Elastic collisions can transfer individual atoms to other spatial modes, reducing the ensemble's purity and the achievable effective spin length. The combined measurements of ΔJ_z and J_{eff} prove that the created many-particle state is in the close vicinity of an ideal symmetric Dicke state.

The measurements can be combined to extract a generalized squeezing parameter $\xi_{\text{gen}}^2 = (N-1)\frac{(\Delta J_z)^2}{\langle J_x^2 \rangle + \langle J_y^2 \rangle - N/2}$ which extends the concept of the spin-squeezing parameter to more general entangled states, including Dicke states [47–49]. Figure 3 (c) presents the measured generalized squeezing parameter as a function of the total number of atoms. Note that the quasi-constant plateau is not statistically significant. At a total of $N = 8000$ atoms, it reaches a value of $-11.4(5)$ dB. This represents the best reported value reached in any atomic system.

In addition to this proof of entanglement, the measured data allow for a quantification of the entanglement depth. Given states with an entanglement depth k, it is possible to deduce a minimal achievable $(\Delta J_z)^2$ for each value of J_{eff}^2 [26]. All states below this minimum must have an entanglement depth larger than k. It can be shown that the states on this boundary $|\Psi\rangle = |\psi\rangle^{\otimes \frac{N}{k}}$ are tensor products of identical k-particle states $|\psi\rangle$. Interestingly, these k-particle states are ordinary spin-squeezed states. Figure 4 shows the boundary in the case of 28-particle entanglement at a total number of 8000 atoms. As a cross-check, random states with 28-particle entan-
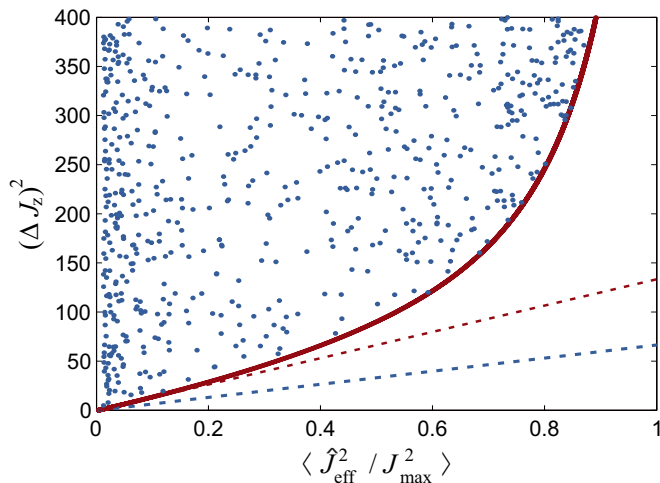
FIG. 4. Detection of k-particle entanglement based on the total spin. The red line marks the boundary for k-particle entangled states with $N = 8000$ and $k = 28$ in the $(\langle \hat{J}_{\text{eff}}^2/J_{\text{max}}^2 \rangle, (\Delta J_z)^2)$-plane. As a cross-check, random states with k-particle entanglement are plotted as blue dots, filling up the allowed region. The criterion of Ref. [29] only detects states that correspond to points below the dashed blue line. An improved linear criterion is gained from calculating a tangent to the new boundary (dashed red line).

glement are plotted in the figure. This confirms that our criterion is optimal and superior to the linear condition of Ref. [29]. Finally, the criterion detects a larger entanglement depth than the criterion given in Ref. [25] when it is applied to spin-squeezed states with minimal experimental noise [26]. It thus outperforms the original criterion in experimentally realistic situations. Beyond spin-squeezing, the criterion is applicable to unpolarized states and thus allows for an optimal evaluation of the entanglement depth of a Dicke-like state as created in our experiments.

Figure 1 (c) shows the entanglement depth of the created state for 8000 atoms. The red lines present the newly derived boundaries for k-particle entanglement. All separable (unentangled) states are restricted to the far left of the diagram, as indicated by the $k = 1$ line. The measured values of $(\Delta J_z)^2$ and $\langle \hat{J}_{\text{eff}}^2/J_{\text{max}}^2 \rangle$ are represented by uncertainty ellipses with one and two standard deviations. The center of the ellipses corresponds to an entanglement depth of 68. With two standard deviations confidence, the data prove that our state has an entanglement depth larger than 28. These numbers are only partly limited by the prepared state itself, but also by the number-dependent detection noise. This detection noise results in a larger measured value of J_z^2 and thus decreases the lower bound for the entanglement depth. This is the largest reported entanglement depth of Dicke-like states. In the future, the measured entanglement depth can be increased by an improved number detection, compensated magnetic field gradients and a

faster spin dynamics.

In summary, we have presented a criterion for the detection of multi-particle entanglement based on a measurement of the ensemble's total spin. In the case of spin-squeezed states, the criterion outperforms the results of previous criteria in experimentally realistic situations. It also extends to more general entangled states, most importantly to Dicke states. We have applied the criterion to detect an entanglement depth larger than 28 in an experimentally created Dicke-like state. The experimental results also allow for a determination of a generalized squeezing parameter of $-11.4(5)$ dB.

[1] R. Horodecki, P. Horodecki, M. Horodecki, and K. Horodecki, Rev. Mod. Phys. **81**, 865 (2009).
[2] O. Gühne and G. Tóth, Phys. Rep. **474**, 1 (2009).
[3] K. Kim, M.-S. Chang, S. Korenblit, R. Islam, E. Edwards, J. Freericks, G.-D. Lin, L.-M. Duan, and C. Monroe, Nature **465**, 590 (2010).
[4] J. Simon, W. S. Bakr, R. Ma, M. E. Tai, P. M. Preiss, and M. Greiner, Nature **472**, 307 (2011).
[5] V. Giovannetti, S. Lloyd, and L. Maccone, Nature Photon. **5**, 222 (2011).
[6] M. Paris and J. Řeháček, eds., Quantum State Estimation, Lecture Notes in Physics, Springer Berlin Heidelberg, Vol. 649 (2004).
[7] A. G. White, D. F. V. James, P. H. Eberhard, and P. G. Kwiat, Phys. Rev. Lett. **83**, 3103 (1999).
[8] C. Schwemmer, G. Tóth, A. Niggebaum, T. Moroder, D. Gross, O. Gühne, and H. Weinfurter, (2014), arXiv:1401.7526.
[9] H. Häffner, W. Hänsel, C. F. Roos, J. Benhelm, D. Chekal kar, M. Chwalla, T. Körber, U. D. Rapol, M. Riebe, P. O. Schmidt, C. Becher, O. Gühne, W. Dür, and R. Blatt, Nature **438**, 643 (2005).
[10] M. Neeley, R. C. Bialczak, M. Lenander, E. Lucero, M. Mariantoni, A. D. O´ Connell, D. Sank, H. Wang, M. Weides, J. Wenner, Y. Yin, T. Yamamoto, A. N. Cleland, and J. M. Martinis, Nature **467**, 570 (2010).
[11] L. DiCarlo, M. Reed, L. Sun, B. Johnson, J. Chow, J. Gambetta, L. Frunzio, S. Girvin, M. Devoret, and R. Schoelkopf, Nature **467**, 574 (2010).
[12] A. Sørensen, L.-M. Duan, J. I. Cirac, and P. Zoller, Nature **409**, 63 (2001).
[13] J. Hald, J. L. Sørensen, C. Schori, and E. S. Polzik,

Phys. Rev. Lett. **83**, 1319 (1999).

[14] M. H. Schleier-Smith, I. D. Leroux, and V. Vuletić, Phys. Rev. Lett. **104**, 073604 (2010).

[15] Z. Chen, J. G. Bohnet, S. R. Sankar, J. Dai, and J. K. Thompson, Phys. Rev. Lett. **106**, 133601 (2011).

[16] R. J. Sewell, M. Koschorreck, M. Napolitano, B. Dubost, N. Behbood, and M. W. Mitchell, Phys. Rev. Lett. **109**, 253605 (2012).

[17] C. Gross, T. Zibold, E. Nicklas, J. Estève, and M. K. Oberthaler, Nature **464**, 1165 (2010).

[18] M. Riedel, P. Böhi, Y. Li, T. Hänsch, A. Sinatra, and P. Treutlein, Nature **464**, 1170 (2010).

[19] C. D. Hamley, C. S. Gerving, T. M. Hoang, E. M. Bookjans, and M. S. Chapman, Nature Phys. **8**, 305 (2012).

[20] C. A. Sackett, D. Kielpinski, B. E. King, C. Langer, V. Meyer, C. J. Myatt, M. Rowe, Q. A. Turchette, W. M. Itano, D. J. Wineland, and C. Monroe, Nature **404**, 256 (2000).

[21] T. Monz, P. Schindler, J. T. Barreiro, M. Chwalla, D. Nigg, W. A. Coish, M. Harlander, W. Hänsel, M. Hennrich, and R. Blatt, Phys. Rev. Lett. **106**, 130506 (2011).

[22] W. Wieczorek, R. Krischek, N. Kiesel, P. Michelberger, G. Tóth, and H. Weinfurter, Phys. Rev. Lett. **103**, 020504 (2009).

[23] R. Prevedel, G. Cronenberg, M. S. Tame, M. Paternostro, P. Walther, M. S. Kim, and A. Zeilinger, Phys. Rev. Lett. **103**, 020503 (2009).

[24] W.-B. Gao, C.-Y. Lu, X.-C. Yao, P. Xu, O. Gühne, A. Goebel, Y.-A. Chen, C.-Z. Peng, Z.-B. Chen, and J.-W. Pan, Nature Phys. **6**, 331 (2010).

[25] A. S. Sørensen and K. Mølmer, Phys. Rev. Lett. **86**, 4431 (2001).

[26] See Supplemental Material, which includes Refs. [50-53].

[27] G. Tóth, C. Knapp, O. Gühne, and H. J. Briegel, Phys. Rev. Lett. **99**, 250405 (2007).

[28] J. Tura, R. Augusiak, A. B. Sainz, T. Vértesi, M. Lewenstein, and A. Acín, arXiv:1306.6860 (2013).

[29] L.-M. Duan, Phys. Rev. Lett. **107**, 180502 (2011).

[30] R. H. Dicke, Phys. Rev. **93**, 99 (1954).

[31] J. Ma, X. Wang, C. Sun, and F. Nori, Phys. Rep. **509**, 89 (2011).

[32] R. Krischek, C. Schwemmer, W. Wieczorek, H. Weinfurter, P. Hyllus, L. Pezzé, and A. Smerzi, Phys. Rev. Lett. **107**, 080504 (2011).

[33] G. Tóth, Phys. Rev. A **85**, 022322 (2012).

[34] P. Hyllus, W. Laskowski, R. Krischek, C. Schwemmer, W. Wieczorek, H. Weinfurter, L. Pezzé, and A. Smerzi, Phys. Rev. A **85**, 022321 (2012).

[35] M. J. Holland and K. Burnett, Phys. Rev. Lett. **71**, 1355 (1993).

[36] A. Chiuri, C. Greganti, M. Paternostro, G. Vallone, and P. Mataloni, Phys. Rev. Lett. **109**, 173604 (2012).

[37] A. Noguchi, K. Toyoda, and S. Urabe, Phys. Rev. Lett. **109**, 260502 (2012).

[38] T. Vanderbruggen, S. Bernon, A. Bertoldi, A. Landragin, and P. Bouyer, Phys. Rev. A **83**, 013821 (2011).

[39] R. Bucker, J. Grond, S. Manz, T. Berrada, T. Betz, C. Koller, U. Hohenester, T. Schumm, A. Perrin, and J. Schmiedmayer, Nature Phys. **7**, 608 (2011).

[40] D. Stamper-Kurn and M. Ueda, Rev. Mod. Phys. **85**, 1191 (2013).

[41] C. Klempt, O. Topic, G. Gebreyesus, M. Scherer, T. Henninger, P. Hyllus, W. Ertmer, L. Santos, and J. J. Arlt, Phys. Rev. Lett. **103**, 195302 (2009).

[42] C. Klempt, O. Topic, G. Gebreyesus, M. Scherer, T. Henninger, P. Hyllus, W. Ertmer, L. Santos, and J. J. Arlt, Phys. Rev. Lett. **104**, 195303 (2010).

[43] C. Gross, H. Strobel, E. Nicklas, T. Zibold, N. Bar-Gill, G. Kurizki, and M. K. Oberthaler, Nature **480**, 219 (2011).

[44] B. Lücke, M. Scherer, J. Kruse, L. Pezzé, F. Deuretzbacher, P. Hyllus, O. Topic, J. Peise, W. Ertmer, J. Arlt, L. Santos, A. Smerzi, and C. Klempt, Science **334**, 773 (2011).

[45] M. Scherer, B. Lücke, G. Gebreyesus, O. Topic, F. Deuretzbacher, W. Ertmer, L. Santos, J. J. Arlt, and C. Klempt, Phys. Rev. Lett. **105**, 135302 (2010).

[46] For small particle numbers, J_{eff} is defined as $J_{\text{eff}}(J_{\text{eff}} + 1) = \langle J_x^2 + J_y^2 \rangle$ with $0 \leq J_{\text{eff}} \leq \frac{N}{2}$. For large particle numbers, we approximate $J_{\text{eff}}^2 \approx \langle J_x^2 + J_y^2 \rangle$.

[47] G. Vitagliano, P. Hyllus, I. L. Egusquiza, and G. Tóth, Phys. Rev. Lett. **107**, 240502 (2011).

[48] G. Vitagliano, I. Apellaniz, I. L. Egusquiza, and G. Tóth, Phys. Rev. A **89**, 032307 (2014).

[49] The new parameter has been used to study the dynamics of the modified Lipkin-Meshkov-Glick model in M. A. Marchiolli, D. Galetti, and T. Debarba, Int. J. Quant. Inf. **11** (2013).

[50] A. Stuart and K. Ord, Kendall's advanced theory of statistics, 6th ed. (Halsted Press, 1994).

[51] Note that the definition of k-particle entanglement in this paper is equivalent to k-producibility as used in the literature. See, for example, O. Gühne, G. Tóth, and H. J. Briegel, New Journal of Physics **7**, 229 (2005). We use the less technical term "k-particle entanglement" for the sake of simplicity.

[52] P. Hyllus, L. Pezzé, A. Smerzi, and G. Tóth, Phys. Rev. A **86**, 012337 (2012).

[53] G. Vitagliano and G. Tóth, in preparation.

SUPPLEMENTAL MATERIAL

S1. ESTIMATION OF VARIANCES

The experimental results of Fig. 3 are based on an estimate of the variance of the total spin of the ensemble. This section shows how these values can be extracted from the raw data. First, the raw data is presented. Second, the statistical treatment for the unbiased estimation of the underlying variance is described. Finally, we show that the variance of J_z results mainly from number-dependent detection noise.

A. Measured probability distribution of J_z and J_α

The number of atoms in the Zeeman levels is measured by standard absorption imaging with an illumination time of $70\,\mu s$ and an intensity of $40\,\mathrm{W/m^2}$. The absolute number of atoms was calibrated [40] and it was confirmed that shot noise fluctuations are observed for a coherent state [see Fig. 3 (a)]. Without the microwave coupling pulse, a measurement of the number of atoms in the Zeeman levels corresponds to a measurement of J_z. While an ideal Dicke state would show no fluctuations at all, we record a finite variance. This finite variance may stem from fluctuations of the number of atoms and from noise in the detection system. Figure S1 (a) shows the histogram of all measured values for J_z with a total number of atoms between 3000 and 7000. The measured distribution is much narrower than the corresponding result for a coherent state. After a $\frac{\pi}{2}$ microwave pulse, it is possible to record the corresponding histogram in the J_x-J_y-plane. Since the microwave has an arbitrary phase difference α from the atomic phases, each measurement projects onto a different axis J_α in the J_x-J_y-plane. The histogram in Fig. S1 (b) thus includes measurements along all possible directions. The histogram shows super-shot-noise fluctuations, yielding a large effective spin length J_{eff}. The presented data can be used to estimate the second moment of the underlying probability distribution.

B. Unbiased estimation of the second moment of the probability distribution

The measurement process creates a finite set of random numbers x_i according to a special, non-Gaussian probability function $P(x)$ [see Fig. S1 (b) as an example]. Such a probability function is well described by its moments $\mu_1 = \int xP(x)dx$ and $\mu_k = \int (x-\mu_1)^k P(x)dx$ for $k \geqslant 2$. The second moment μ_2, which presents the central quantity of interest within our work, can be estimated straightforwardly from the measurements as shown below. However, the variance of this estimate is more diffi-
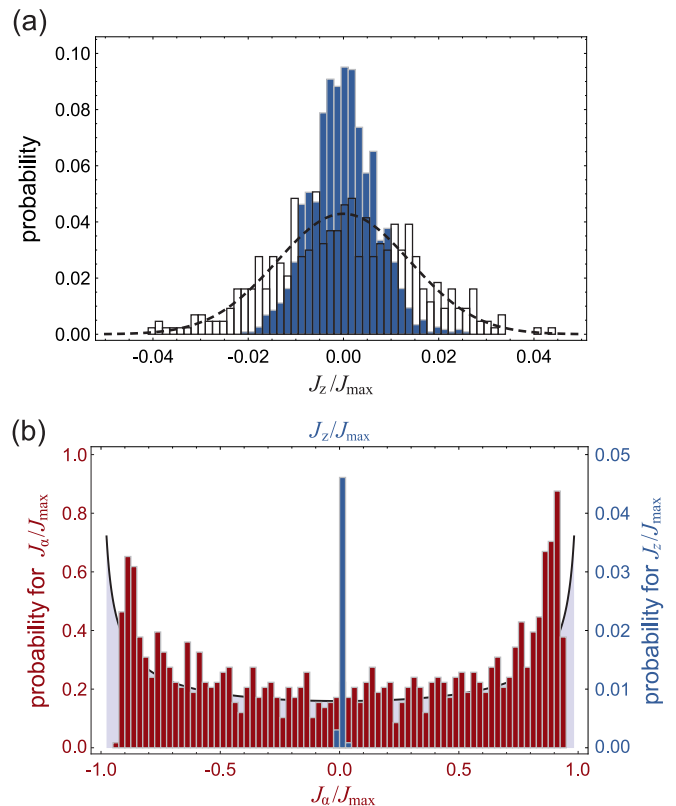
(a)

(b)

FIG. S1. Histograms of the recorded spin measurements. (a) The accumulated measurements of J_z are shown for a Dicke-like state (solid blue columns) and a coherent state (open columns). The distribution of the Dicke-like state is much narrower than the distribution of the coherent state. The latter is very close to a binomial distribution with shot noise fluctuations (dashed line). We corrected for a small offset between the two distributions. (b) The accumulated measurements of J_α are shown for a Dicke-like state (solid red columns). The distribution compares well to the distribution of a perfect Dicke state (solid grey line with shading). It is much wider than the sub-shot-noise distribution of J_z (solid blue columns).

cult to deduce and has previously been gained from split samples [16]. In this section, we present a formula for an unbiased estimate of this variance (called second moment variance estimator, SMVE), allowing for the calculation of correct error bars for the central result of our work [see Fig. 1 (c)].

For a given sample of n independent measurements according to the probability function $P(x)$, it is possible to calculate the sample moments

$$m_1 = \frac{1}{n} \sum_{i=1}^{n} x_i,$$

$$m_2 = \frac{1}{n} \sum_{i=1}^{n} (x_i - m_1)^2,$$

$$m_4 = \frac{1}{n} \sum_{i=1}^{n} (x_i - m_1)^4.$$

The expectation value of m_2 is easily calculated to be

$$\langle m_2 \rangle = \frac{n-1}{n} \mu_2.$$

It is thus possible to define an unbiased estimator for μ_2:

$$\hat{\mu}_2 = \frac{n}{n-1} m_2.$$

This estimate shows statistical fluctuations which are described by the variance of $\hat{\mu}_2$,

$$\begin{aligned}
\text{var}(\hat{\mu}_2) &= \frac{n^2}{(n-1)^2} \text{var}(m_2) \\
&= \frac{n^2}{(n-1)^2} \left(\langle m_2^2 \rangle - \langle m_2 \rangle^2 \right) \\
&= \frac{n^2}{(n-1)^2} \langle m_2^2 \rangle - \mu_2^2. \quad \text{(S1)}
\end{aligned}$$

Thus, the problem of finding an estimator for $\text{var}(\hat{\mu}_2)$ reduces to finding an estimator for μ_2^2. Hence, we calculate the expectation values $\langle m_2^2 \rangle$ and $\langle m_4 \rangle$ by using augmented and monomial symmetric functions (see Ref. [50] p. 416).

$$\langle m_2^2 \rangle = \frac{(n-1)^2}{n^3} \mu_4 + \frac{(n-1)(n^2-2n+3)}{n^3} \mu_2^2$$

$$\langle m_4 \rangle = \frac{n^3-4n^2+6n-3}{n^3} \mu_4 + \frac{3(n-1)(2n-3)}{n^3} \mu_2^2$$

This linear system of equations can be solved to yield an estimator for μ_2^2. By substituting this in Eq. (S1), we obtain the final result for the SMVE,

$$\text{var}(\hat{\mu}_2) = \frac{n}{(n-3)(n-2)} m_4 - \frac{n(n^2-3)}{(n-3)(n-2)(n-1)^2} m_2^2.$$

The SMVE allows for a direct calculation of the error bars from the moments of the recorded sample without any assumption on the shape of the probability distribution.

Figure S2 shows the result of a Monte-Carlo simulation to demonstrate the application of the SMVE. We generate random numbers according to a probability function
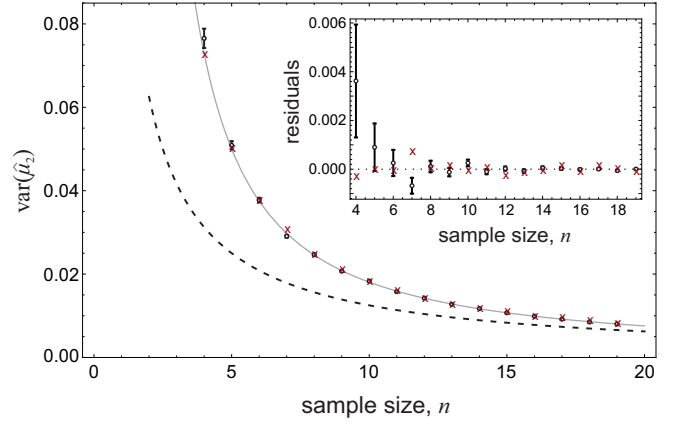

FIG. S2. Application of the SMVE to generated random numbers. We have generate random numbers according to a probability function $P(x)$. For each sample size n, we have applied the SMVE to 10^4 samples. The open circles present the mean of the calculated SMVEs with their statistical uncertainties. These results compare well to the directly calculated variance of the 10^4 sample variances (red solid dots). It is statistically equal to the prediction $\text{var}(\hat{\mu}_2) = \frac{1}{n}\mu_4 - \frac{n-3}{n(n-1)}\mu_2^2$ and completely incompatible with the naive guess $\text{var}(\hat{\mu}_2) \approx \frac{1}{n}(\mu_4 - \mu_2^2)$ (dashed line).

$P(x) = \frac{1}{\pi}\sqrt{\frac{1}{1-x^2}}$, similar to Fig. S1 (b), and accumulate samples of variable size. The SMVE is applied to 10^4 samples of each size, yielding estimates for $\text{var}(\hat{\mu}_2)$. Figure S2 shows that these estimates approximate the directly calculated variance of the 10^4 sample variances very well. It is statistically equal to the prediction gained solely from the shape of the probability distribution.

In summary, the statistical treatment allows for a correct evaluation of the second moment of the underlying probability function and its uncertainty.

C. Estimation of the detection noise

The second moment gained from the experimental measurements via the statistical treatment above is a combination of the variance $(\Delta J_z)^2$ of the atomic many-particle state and the detection noise. The detection noise comprises an atom-independent part which is dominated by the photoelectron shot noise on the camera pixels and an atom-dependent part. The atom-independent noise was measured continuously during the data acquisition by analysing images without atoms. Since we are interested in an estimate for $(\Delta J_z)^2$, the data in Fig. 3 (a) are corrected for the atom-independent noise.

The atom-dependent detection noise results from fluctuations of the photoelectrons counted on the camera pixels which are stronger at a large number of atoms. Additionally, a change in the number of counted photoelectrons has a larger effect on the estimated number of
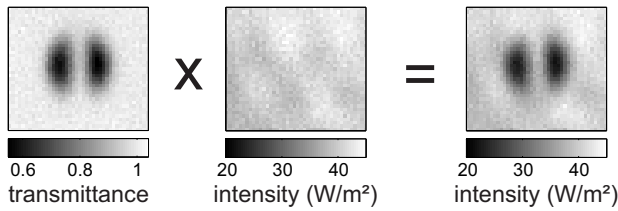
FIG. S3. Creation of an artificial absorption image. The optical transmittance of an idealized atomic cloud is calculated from an average of many experimental absorption images. A typical detection image without atoms is multiplied by the optical transmittance to gain a synthetic absorption image with adjustable number of atoms.

atoms at high column densities resulting in an increased sensitivity at a large number of atoms. This noise source is not independent of the atomic noise and it is thus not legitimate to subtract it. Nevertheless, we estimate the approximate strength of these fluctuations for comparison with our results. For this purpose, we calculate the mean optical transmittance from many experimental realizations (see Fig. S3) to approximate an ideal atomic cloud without atom number fluctuations. This optical transmittance image is adjusted to represent clouds with different numbers of atoms. We synthesize absorption images by multiplying empty detection images with the gained transmittance images. These artificial absorption images provide a measure of the atom-dependent detection noise since they do not contain any atom number fluctuations by construction. The resulting estimate for the atom-dependent detection noise is shown in Fig. 3 (a) (dashed line). Although it underestimates the effect of photoelectron shot noise for strongly depleted absorption images, it nevertheless explains the major part of the measured variance $(\Delta J_z)^2$.

S2. BOUNDARIES FOR GENUINE k-PARTICLE ENTANGLEMENT

This section presents a method for the determination of the entanglement depth based on the measurement of $\langle J_x^2 + J_y^2 \rangle$ and $(\Delta J_z)^2$. With this method, we determine the allowed regions for k-particle entanglement in Fig. 1 (c). Section S2 A provides a numerical method to calculate the boundaries. In Sec. S2 B, we present the entanglement criterion with a closed formula, and we discuss that it applies to pure states, mixed states and mixed states with a varying particle number. Finally, Sec. S2 C presents a comparison with the original spin-squeezing criterion of Ref. [24]. We show that our criterion detects a larger entanglement depth for extreme spin-squeezed states in the presence of minimal noise.

A. Numerical determination of the boundaries

The following numerical method can be used to determine the allowed region in the $(\langle J_x^2 + J_y^2 \rangle, (\Delta J_z)^2)$-space for quantum states with at most k-particle entanglement for a given particle number N [51]. We consider states of the form

$$|\Psi\rangle = \otimes_{n=1}^{M}|\psi^{(n)}\rangle, \qquad (S2)$$

where $|\psi^{(n)}\rangle$ is the state of the nth non-separable subset containing k_n qubits and $k_n \leqslant k$. In total, there are M non-separable subsets. Here, "qubit" refers to individual pseudo-spin-$\frac{1}{2}$ atoms in the experiment. We define the collective operators

$$J_l := \sum_{n=1}^{M} j_l^{(n)}$$

for $l = x, y, z$, where $j_l^{(n)}$ denotes the components of the k_n-particle spin operators and act on the nth non-separable subset of qubits. Note that we consider $k_n = k$ in the main text, whereas here, we extend our discussion to the general case $k_n \leqslant k$.

The total variance $(\Delta J_z)^2$ is given by the sum of the variances of the k_n-particle spin operators

$$(\Delta J_z)^2 = \sum_n (\Delta j_z^{(n)})^2. \qquad (S3)$$

On the other hand, for a state of the form (S2)

$$\langle J_x^2 + J_y^2 \rangle = \sum_n \langle \left(j_x^{(n)} \right)^2 + \left(j_y^{(n)} \right)^2 \rangle$$
$$+ \sum_{m \neq n} \left(\langle j_x^{(m)} \rangle \langle j_x^{(n)} \rangle + \langle j_y^{(m)} \rangle \langle j_y^{(n)} \rangle \right).$$

Since for non-negative values $\{x_l\}_{l=1}^{L}$ and positive integer L we have

$$\sum_{l \neq m} x_l x_m \leqslant (L-1) \sum_l x_l^2,$$

we obtain

$$\langle J_x^2 + J_y^2 \rangle \leqslant \sum_n \langle \left(j_x^{(n)} \right)^2 + \left(j_y^{(n)} \right)^2 \rangle$$
$$+ (M-1) \sum_n \left(\langle j_x^{(n)} \rangle^2 + \langle j_y^{(n)} \rangle^2 \right). \qquad (S4)$$

For simplicity, we assume that N is divisible by k. In this case, states of the form

$$|\Psi\rangle = |\psi\rangle^{\otimes \frac{N}{k}} \qquad (S5)$$

saturate the inequality (S4), where $|\psi\rangle$ is a k-qubit state. Due to convexity arguments, it is sufficient to

look for states of the form (S5) to calculate the boundary points. A boundary point can be obtained for a given $X = (\Delta J_z)^2$ from

$$\langle J_x^2 + J_y^2\rangle(X) = \max_{|\Psi\rangle, \frac{N}{k}(\Delta j_z)^2 = X} \left[\frac{N}{k}\langle j_x^2 + j_y^2\rangle_{|\psi\rangle} \right.$$
$$\left. + \left(\frac{N}{k} - 1\right)\frac{N}{k}\left(\langle j_x\rangle_{|\psi\rangle}^2 + \langle j_y\rangle_{|\psi\rangle}^2\right)\right]. \quad (S6)$$

Thus, a constrained optimization for a given $(\Delta j_z)^2_{|\psi\rangle}$ over $|\psi\rangle$ has to be performed. This can be simplified further as follows. For even k, the states at the boundary can be sought in the form (S5), where $|\psi\rangle$ is the ground state of the spin-squeezing Hamiltonian

$$h(\lambda) = j_z^2 - \lambda j_x. \quad (S7)$$

Thus, an optimal state $|\psi\rangle$ is obtained from spin squeezing [13]. Note that the ground state of $h(0)$ is degenerate. In this case, the symmetric ground state has to be chosen, i.e., the symmetric Dicke state with $\langle j_z\rangle = 0$.

Hence, the boundary points can be obtained for even k as a function of a single real parameter λ as

$$\langle J_x^2 + J_y^2\rangle(\lambda) = \left[\frac{N}{k}\langle j_x^2 + j_y^2\rangle_{|\psi\rangle(\lambda)} \right.$$
$$\left. + \left(\frac{N}{k} - 1\right)\frac{N}{k}\left(\langle j_x\rangle_{|\psi\rangle(\lambda)}^2 + \langle j_y\rangle_{|\psi\rangle(\lambda)}^2\right)\right],$$
$$(\Delta J_z)^2(\lambda) = \frac{N}{k}(\Delta j_z)^2_{|\psi\rangle(\lambda)},$$

where $|\psi\rangle(\lambda)$ is the ground state of $h(\lambda)$. This also means that states of the form $|\psi\rangle^{\otimes\frac{N}{k}}(\lambda)$ correspond to points on the boundary. Since $\langle j_z\rangle_{|\psi\rangle(\lambda)} = 0$, we have $\langle J_z\rangle = 0$ for the states on the boundary mentioned above. Any state beyond the boundary is at least $(k+1)$-particle entangled.

B. Proof for general states with a large number of particles

In the previous section, we have presented a numerical method to calculate the boundary for k-particle entangled states assuming that the state is a tensor product of k-qubit pure states and the particle number is fixed. It is possible to prove that these boundaries are valid for general states (S2) with $k_n \leqslant k$.

To obtain a closed formula for the boundary, we employ the definition [13]

$$F_j(X) := \frac{1}{j}\min_{\frac{\langle j_x\rangle}{j} = X}(\Delta j_z)^2.$$

The spin-squeezing criterion for k-particle entangled states is given as

$$(\Delta J_z)^2 \geqslant J_{\max}F_{\frac{k}{2}}\left(\frac{\sqrt{\langle J_x\rangle^2 + \langle J_y\rangle^2}}{J_{\max}}\right). \quad (S8)$$

Equation (S8) is valid for any tensor product of states of the form (S5) with $k_n \leq k$ [13,S3].

Moreover, for pure k-particle entangled states it is straightforward to show that

$$\langle J_x^2 + J_y^2\rangle \leqslant J_{\max}(\tfrac{k}{2} + 1) + \langle J_x\rangle^2 + \langle J_y\rangle^2. \quad (S9)$$

Hence, using the properties of $F_j(X)$, for states with k-particle entanglement,

$$(\Delta J_z)^2 \geqslant J_{\max}F_{\frac{k}{2}}\left(\frac{\sqrt{\langle J_x^2 + J_y^2\rangle - J_{\max}(\frac{k}{2} + 1)}}{J_{\max}}\right) \quad (S10)$$

holds. Naturally, we can use the formula only if the expression under the square root is positive. Otherwise, the lower bound on $(\Delta J_z)^2$ is trivially zero. For large N and $k \ll N$, the first term under the square root in Eq. (S10) is $\sim N^2$, while the second one is $\sim N$. Thus, we obtain approximately

$$(\Delta J_z)^2 \gtrsim J_{\max}F_{\frac{k}{2}}\left(\frac{\sqrt{\langle J_x^2 + J_y^2\rangle}}{J_{\max}}\right). \quad (S11)$$

Note that, since $F_j(x) \leqslant \frac{1}{2}$, a sub-Poissonian variance, i.e., $(\Delta J_z)^2 < \frac{N}{4}$ is required to detect multi-particle entanglement.

The inequality (S10) can be used to quantify the entanglement depth of pure states. It gives the same boundary for k-particle entangled states as the method of Sec. S2 A. It can also be shown that our criterion holds not only for pure states, but also for general mixed states [52]. Moreover, it can be generalized to the experimentally important case of mixed states with a fluctuating total number of particles. Since the total proof exceeds the scope of this publication, it will be published elsewhere [53].

C. Comparison with the spin-squeezing criterion

Our criterion reliably detects the entanglement depth of Dicke states. In particular, it detects the symmetric Dicke state with $\langle J_l\rangle = 0$ for $l = x, y, z$ as fully N-particle entangled, since the inequality (S10) with $k = N - 1$ is violated. In this section, we show that our criterion is also valuable for the evaluation of spin-squeezed states, since it outperforms the criterion of Ref. [24] in the presence of noise.

In order to compare the performance of the two criteria, we consider the ground states of the spin-squeezing Hamiltonian

$$H(\Lambda) = J_z^2 - \Lambda J_x, \quad (S12)$$

for $N = 4000$ spin-$\frac{1}{2}$ particles. For $\Lambda = \infty$, the ground state is fully polarized. For $\Lambda = 0$, it is the symmetric
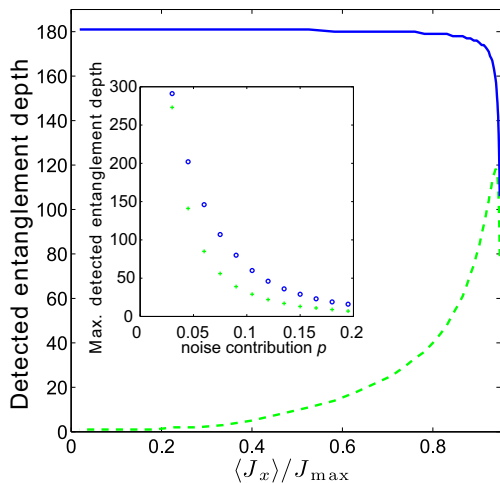
FIG. S4. Comparison with the spin-squeezing criterion. The graph shows the entanglement depth detected by the condition (S10) (solid line) and the spin-squeezing condition (S8) (dashed line) for $N = 4000$ spin-$\frac{1}{2}$ particles with additive white noise to account for imperfections. For states that are not completely polarized, Eq. (S10) detects a considerably larger entanglement depth. The inset shows that the maximal detected entanglement depth depending on the noise contribution is larger for our criterion (circles) than for the spin-squeezing criterion (crosses) if some very small noise is present.

Dicke state. In principle, such states are detected by the spin-squeezing criterion of Ref. [24] as fully N-particle entangled for all $\Lambda > 0$. However, this statement only holds for ideal pure states. In experimentally realistic situations, small noise contributions are always expected, especially for the case of large numbers of particles as considered here. While the criterion of Ref. [24] becomes extremely sensitive to noise for strongly squeezed states, our criterion is much more robust.

We account for these small noise contributions by mixing the density matrix of the ideal spin-squeezed state ρ_{id} with a noisy state ρ_n. The noisy state is chosen such that each atom is in an incoherent 50/50 mixture of its two spin states. For a quantitative comparison, we estimate the entanglement depth of the state $\rho = (1-p)\,\rho_{id} + p\,\rho_n$ with a noise contribution of $p = 0.05$. Fig. S4 shows the detected entanglement depth for the spin-squeezing criterion (S8) and our criterion (S10). For strongly squeezed states, where $\langle J_x \rangle \ll J_{max}$, our criterion detects a large entanglement depth, while the result of the method described in Ref. [24] tends to zero. The robustness against noise exhibited in this example is a general property and is independent of the exact type of noise.

In summary, our criterion detects the entanglement depth of both spin-squeezed states and more general states in experimentally realistic situations. Most prominently, it is ideally suited for the characterization of Dicke states, as produced in our experiments.